Windblown sand action on civil structures: Definition and probabilistic modelling

Engineering Structures 178 (2019) 88–101

Contents lists available at ScienceDirect

Engineering Structures

journal homepage: www.elsevier.com/locate/engstruct

Windblown sand action on civil structures: Definition and probabilistic modelling

Lorenzo Raffaele*, Luca Bruno

Politecnico di Torino, Department of Architecture and Design, Viale Mattioli 39, I-10125 Torino, Italy
Windblown Sand Modeling and Mitigation Joint Research Group, Italy

ARTICLE INFO

Keywords:
Windblown sand
Sand action
Sand limit states
Probabilistic method
Reliability analysis
Time-variant
Monte Carlo

ABSTRACT

The accurate prediction of windblown sand effects on structures and infrastructures is fundamental for their design and performance assessment in desert and coastal regions. Windblown sand occurs in the form of moving sand dunes, sand drift, sand erosion, accumulation, and avalanching around built structures. Windblown sand is here defined as an environmental variable action, analogously to wind or snow actions. We categorize its effects into Sand Ultimate Limit States and Sand Serviceability Limit States. We propose a framework to assess windblown sand action by means of a probabilistic method because of the inborn variability of the phenomenon. The proposed method is useful for the design of both structures and infrastructures and of sand mitigation measures. It allows to evaluate characteristic values of the sand action and assess related characteristic times of failures. In order to prove its technical feasibility, the proposed framework is then applied to a desert railway because of the particular sensitivity of such kinds of infrastructures to windblown sand action.

1. Introduction

The design of structures and infrastructures needs to face environmental actions. Among them, wind action, snow action, and their interaction have gained wide attention in structural design. Wind action on structures and its effects have been extensively investigated from the pioneering studies of Davenport [1] and the seminal book of Simiu and Scanlan [2]. Snow loads on structures have been defined on the basis of nation and international research project, such as the European Snow Load Research Project [3]. Wind and snow interaction has been investigated in a number of scientific studies in the form of snow drift (e.g. [4,5]) and ice accretion (e.g. [6]). National and international standards and guidelines now regulate wind action (e.g. [7]), snow action (e.g. [8]), snow drift effects on simple roofs (e.g. [8]), design criteria against windblown snow for roads and highways [9], and atmospheric icing of structures [10]. In this framework, climate change has a strong impact on environmental conditions (e.g. [11,12]). As a result, environmental actions needs to be updated in order to properly design new structures and grant the reliability of the existing ones. From this perspective, research activity is recently addressing such issue for both wind action [13] and snow loads [14].

This study refers to *windblown sand as an environmental action* by analogy with wind and snow actions. The analogy above was early recognized in a phenomenological and physical modelling perspective by e.g. [15,16], where both sand grains and snow flakes are intended as particulate materials. Analogously to snow drift, windblown sand results from the interaction between wind and sand, and implies sand erosion, transport, sedimentation and avalanching around any kind of built structure. To our best knowledge, such an analogy has not been transferred to structural engineering in order to define windblown sand action. This entails that windblown sand action and its effects on civil structures and infrastructures are almost completely overlooked in structural engineering, despite the wide range of induced deficiencies, and the need of ad hoc engineering studies and solutions early recognized by e.g. [17,18]. Being structural engineers usually unfamiliar with windblown sand action, in the following we shortly introduce the geographical location of the regions potentially susceptible to windblown sand, its effects on structures and infrastructures, the categorization of the windblown sand action and the way in which existing codes and guidelines deal with it, and some of the design solutions proposed so far.

The worldwide *geographical location* of the regions potentially susceptible to windblown sand is shown in Fig. 1. Such regions are coastal zones with well developed dune systems [19] and arid and desert regions with active sand sources, i.e. desert areas covered with sand with little or no vegetation [20]. Windblown sand-prone zones take up about

* Corresponding author.
E-mail address: lorenzo.raffaele@polito.it (L. Raffaele).
URL: http://www.polito.it/wsmm (L. Raffaele).

https://doi.org/10.1016/j.engstruct.2018.10.017
Received 19 June 2018; Received in revised form 4 October 2018; Accepted 8 October 2018

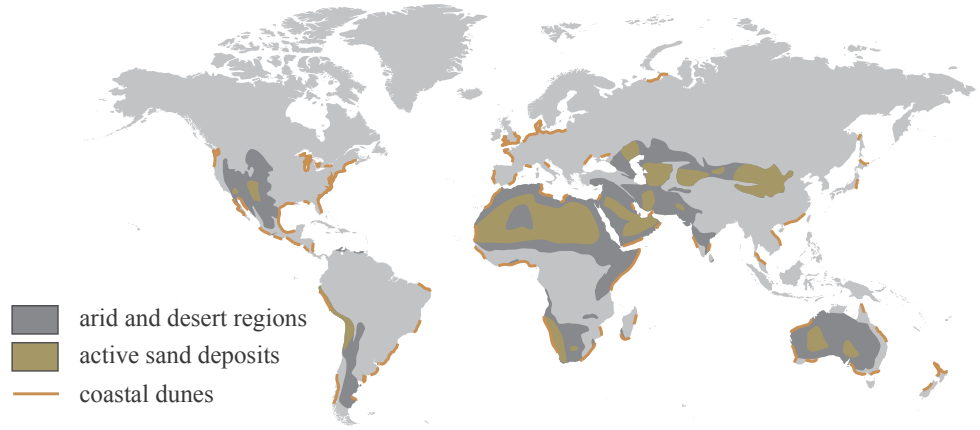

Fig. 1. Geographical location of the regions potentially susceptible to windblown sand. Coastal dunes redrawn from [19], active sand deposits redrawn from [20].

one fifteenth of the Earth's land surface. These zones are increasingly hosting human activities, such as transport, industrial, mineral, and residential ones. The hazards induced by windblown sand in drylands and along coastal zones are reviewed in the field of Earth sciences by [21,22], respectively.

The *effects of windblown sand action* are highly bound to the scale and the nature of the structure it interacts with. Windblown sand can act at the scale of a single built structure [23] (Fig. 2c and e), at the urban scale [24] (Fig. 2b and d), and/or at the infrastructure scale [25] (Fig. 2g–j). The geographical location of some remarkable documented case of windblown sand attacking built structures is reported in Fig. 2(a). Among coastal sites, it is worth mentioning severe windblown sand affecting each year Bayshore district in Waldport, Oregon [22], moving dunes at Silver Lake shore in Michigan [26], the half sand buried Shoyna village in Russia, windblown sand affecting the North Sea costs in northern Europe [27] (Fig. 2b and c). Among desert sites, it is worth mentioning the towns of Nouakchott in Mauritania (Fig. 2d), In-Salah in Algeria [28] (Fig. 2e), Shiquanhe in Tibet [29], and

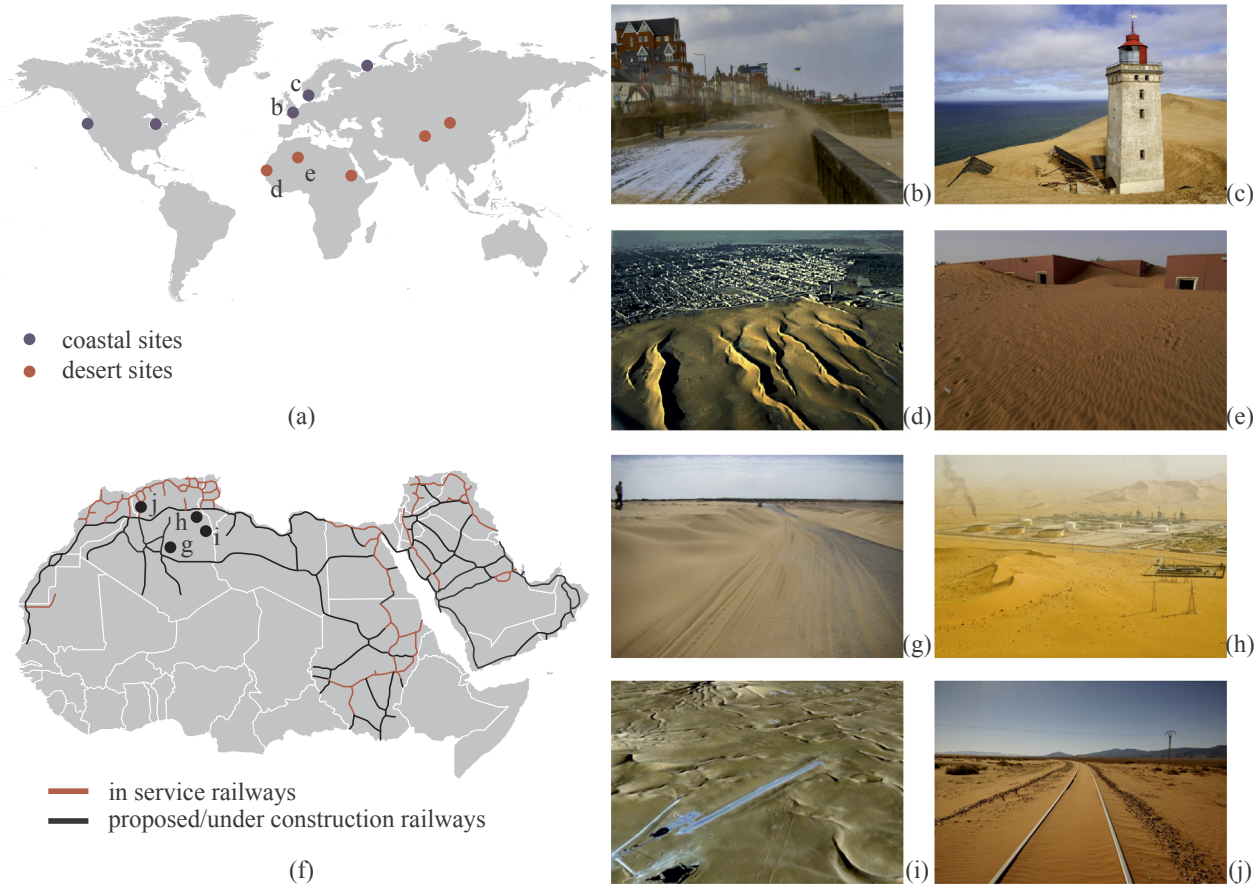

Fig. 2. Examples of civil structures affected by windblown sand (a): Cleethorpes, UK (b, explicit publishing permission from the owner of the photo: Duncan Young [39]), Rubjerg Knude lighthouse, Denmark (c, explicit publishing permission from the owner of the photo: Andreas Lembke), Nouakchott, capital of Mauritania (d, Landsat 1565-10032-6, 1974), In-Salah, Algeria (e, from Panoramio). Examples of civil infrastructures affected by windblown sand in MENA region (f): road (g, explicit publishing permission from the owner of the photo: Nouar Bolghobra [40]), oil refinery (h, publishing permission under Creative Commons Attribution License from Stefano F, www.flickr.com/photos/stefof), airport runway (i, from Google Earth), railway (j).

Dunhuang in China [30], but also archaeological sites, e.g. the Kharga Oasis monuments in Egypt [31], the Meroe Pyramids in Sudan, the Mogao Grottoes in China [30]. Railways crossing deserts or arid environments shall be designed by devoting particular attention to windblown sand environmental action. Their interaction with windblown sand is of particular engineering interest because of both their extension and technical complexity. Indeed, windblown sand action translates into several forms given their components in civil works, track superstructure, rolling stock and signalling technologies. New ultra-long transnational railway megaprojects are currently being planned. Fig. 2(f) depicts railways currently in service, in construction and future proposed in Middle East and North Africa (MENA) region. In general, sand action on railway infrastructures leads to incremental costs in infrastructure management, e.g. service suspension, loss of capacity and increased maintenance costs [32], but also to destructive failures, such as train derailment [33–35]. Among other civil infrastructures, windblown sand particularly affects roads and highways [17] (Fig. 2e), pipelines and refineries [36] (Fig. 2h), industrial facilities [37], and airports [38] (Fig. 2i).

The *categorization of the windblown sand action* is missing both in scientific literature and standards. The only remarkable exception is given by the Algerian snow and wind code ([41], Sect. 7): the sand loads are considered as a variable, direct, fixed, static action in analogy to snow loads; they are viewed as resulting from accumulation of sand transported by the wind; the sand zoning map of the Country is given, analogously to wind and snow ones; global and local distributed vertical loads are provided for flat and multi-span roofs, respectively. The windblown sand accumulation does not translate only into static loads directly applied on structures, but also into indirect actions, once more in analogy to snowdrift, wind-driven ice accretion and other environmental influences that affect durability, impair the performance of the built structure/infrastructure and results in frequent maintenance [42]. In spite of the analogy between sand and snow action, it is useful to put the stress on some differences. i. Wind is necessary to sand lifting, subsequent accumulation and resulting action, while gravity forces in still air are sufficient to drive snowflakes free fall. ii. Sand accumulation can result in both vertical loads on roofs and unprotected floors, and in horizontal loads on wall or diaphragms, because its low cohesion and high density. Conversely, snow accumulation mainly implies vertical load only, while low horizontal static loads results from low cohesion and low snow density (fresh snow), or vice versa (old snow). iii. Sand avalanching results in a quasi-steady load, because of the progressive low-speed sliding of the superficial layer only, while snow avalanching results in an impact load because of massive high-speed sliding. iv. The sand accumulation and related action is monotonically increasing in time, if periodic removal is not included in the maintenance plan, while accumulated snow can be subjected to melting.

A number of *design solutions* have been proposed in literature in order to mitigate windblown sand effects. The authors recently classified solutions adopted along railways, also called Sand Mitigation Measures (SMMs), into an innovative Source-Path-Receiver scheme [25]. However, the same categorization also applies to the general case of SMMs around built structures (Fig. 3a). Such scheme is conceived on the basis of SMMs location with respect to the windblown sand path and on their working principles. Source design solutions are located on the sand source and are independent on the structure type. They are mainly intended to reduce the sand erosion from the source. Fig. 3(b) shows polyethylene-net checkerboards applied on a sand source. Path design solutions are located along the windblown sand path splitting it into upwind and downwind strips. They are intended to trap windblown sand by promoting sand sedimentation around the SMM, and away from the protected structure. In turn, sand sedimentation is obtained by the aerodynamic characteristics of the SMM, that locally modifies the wind flow and decreases the wind speed. The path SMM trapping efficiency shall be understood as the ratio between the trapped sand and the incoming sand. The efficiency mainly depends on the SMM aerodynamics and on the time-varying sand accumulation volume, that has a detrimental effects on the SMM aerodynamic performances in turn [44]. Hence, periodic sand removal is mandatory for path SMMs. Path SMMs usually consists of ditches or dykes obtained by earthworks, porous structural fences [45,46] or solid barriers [47]. Fig. 3(c) shows a urban-scale path design solution consisting of V-shaped deflecting solid barriers built upwind the In-Salah oasis town in central Algeria. Receiver design solutions are located next to the structure or, alternatively, are part of the structure itself. They are mainly intended to promote the wind-induced erosion and transport of the sand far from the structure. Fig. 3(d) shows a low-rise pier-mounted building in In-Salah, where bottom openings aim at preventing sand sedimentation at the ground level. The same working principle has been adopted in [48] to lower snow accumulation around an antarctic base.

In the light of the state-of-art briefly introduced above, let us schematically resume some highlights. i. A high and growing number of civil structures and infrastructures are built in desert and coastal regions. ii. The design, analysis and performance assessment of such structures and infrastructures face to windblown sand action remain at their infancy and in the realm of empiricism. iii. Despite pioneering ad hoc sand studies for specific projects, a systematic and comprehensive problem setting in an engineering perspective is still missing.

In this study, we aim at contributing to this new research field by a general modelling framework able to evaluate the windblown sand action on a generic built structure, and to assess the performances of design solutions, if required to reduce the sand effects. The modelling framework is necessarily conceived in probabilistic terms, in order to account for inborn uncertainties of both wind and sand [49]. The sand action is assessed on the basis of a time-variant reliability analysis, because of the slowly increasing sand accumulated volume and resulting action. The analysis is intended to predict the characteristic time of failure referred to any levels of performance of the structure and/or SMM.

The paper develops accordingly to the above objectives through the following sections. The main phenomenological features of the windblown sand are discussed in Section 2 from the engineering perspective. Section 3 briefly recalls windblown Sand Limit States of built structures and infrastructures. Section 4 introduces the proposed framework to assess windblown sand action in probabilistic terms. The approach is applied in Section 5 to a case study dealing with a railway protected by two different kind of solid barriers. Obtained results are discussed and barrier performances are compared. Finally, Section 6 outlines conclusions and perspectives.

2. Windblown sand phenomenological analysis

In the following, a concise phenomenological analysis of windblown sand is given to ground its successive modelling. First, the features of windblown sand erosion and transport far from any built structure, i.e. at sand source and along the upwind sand path (Fig. 3a) are discussed in Section 2.1. Secondly, Section 2.2 describes windblown sand erosion, sedimentation and avalanching around built structures.

2.1. Windblown sand far from built structures

Windblown sand transport is characterized by many modes of particles motion depending on the grain diameter d (see Fig. 4b), i.e. suspension ($d < 0.07$ mm), saltation ($0.07 < d < 0.5$ mm), and creep ($d > 0.5$ mm). Among all transport mechanisms, saltation mainly contributes to the total transported sand mass [51]. Saltation is triggered by wind shear stresses on the sand surface, that depends in turn on the wind velocity gradient. Saltation follows from the bouncing of sand grains on the sand bed in the wind direction, and finally results in a horizontal flux of sand mass [52]. The saltation layer along a flat sandy plane lies in the lower boundary of the atmospheric boundary layer. Its mean height is approximately equal to 5–20 cm, while the maximum

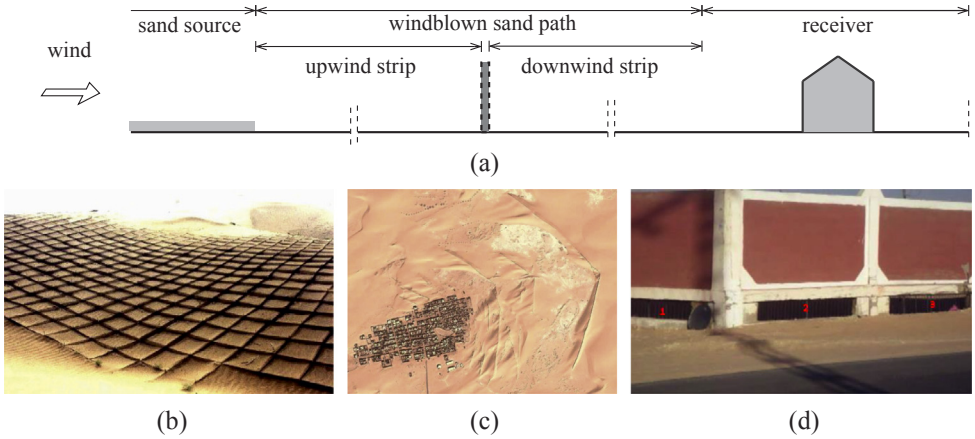

Fig. 3. Design solution against windblown sand action. Conceptual scheme (a). Source design solution: polyethylene-net checkerboards for sand dune stabilization in China (b, reprinted from [43], with permission from Elsevier). Path design solution: deflecting barriers in In-Salah (c, from Google Earth). Receiver design solution: low-rise pier-mounted building in In-Salah (d, explicit publishing permission from the owner of the photo: Nouar Bolghobra [40]).

height may reach ten times the mean saltation height [53]. The instantaneous magnitude of windblown sand flux transported by saltation is of the order of 1 g $m^{-2}s^{-1}$ for moderate wind speed. The cumulate amount of sand transported by wind over one year and per crosswind lineal meter, i.e. the so-called resultant drift potential magnitude [54], can reach 25 $m^3m^{-1}yr^{-1}$, i.e. about 45 tons $m^{-1}yr^{-1}$, in windy and sandy regions (see e.g. [49]).

2.2. Windblown sand around built structures

The windblown sand action results from the wind flow field and sand morphodynamics around the affected structure. Some real world case studies are collected in Fig. 5, left column. For each of them, the local wind field topology is schematized by referring to the huge literature in the field of surface-mounted bluff body aerodynamics (e.g. [55,56], Fig. 5, central column). Correspondingly, the local sand morphodynamics around built structures are depicted by translating the experimental studies on natural obstacles, such as boulders and clumps of vegetation (e.g. [57] and references therein, Fig. 5, right column). The case studies are selected as examples of the three main aeolian phenomena arising around built structures: erosion, sedimentation, and avalanching.

Erosion implies scour around built structures. Scour is a well known effect in structural, fluvial and coastal engineering. Indeed, it takes place in a variety of design scenarios, e.g. around bridge piers [65], or around marine and offshore structures [66]. A remarkable three-dimensional aeolian scour is shown in Fig. 5(a) around one of the Meroe pyramids in Sudan. The wind flow pattern around an isolated pyramid is characterized by an upwind horseshoe vortex (Fig. 5b), similarly to others bluff bodies and wind incidences (e.g. [67], Fig. 5m). Such a vortex results from the interaction between the atmospheric boundary layer and the boundary layer along the frontal and side surfaces of the mounted body. The reversed flow close to the ground induces sand erosion in front and around the pyramid (Fig. 5c). Sedimentation only occurs around the wake midline, where vortices of opposite sign are close to each other [59].

Fig. 5(d) shows a simpler example of two-dimensional aeolian scour at the toe of a 2 m high fence, 3 months after its installation [60]. The bottom opening induces the well known Venturi effect, i.e. the acceleration of the wind flow across the gap (Fig. 5e). It involves local erosion of the sedimented sand at the fence foundation, and local sedimentation of the transported sand where the flow decelerates [68] (Fig. 5f).

An analogous Venturi effect and related erosion take place across the gap between two solid barriers (plan view, Fig. 5h), if the depth/gap ratio D/G is much lower than unit. Once more, sand sedimentation occurs where the wind speed decreases, i.e. downwind the barrier free end [61] and in the wake far from the gap [62] (Fig. 5i).

Sedimentation and progressive sand accumulation around structures can occur under different circumstances. Fig. 5(g) shows the partial obstruction of culverts across a railway embankment. Unlike the gapped barrier above, here the D/G ratio is higher than unit. The separation bubbles just downstream the duct leading edges act as a virtual convergent/divergent segment, and induce the flow deceleration along the remaining length of the duct, other than in the culvert far wake (Fig. 5j). A massive sand accumulation along the duct and the culvert obstruction follows, in addition to the sedimentation at the shoulder recirculation regions and in the wake far from the culvert (Fig. 5k).

Fig. 5(l) shows the accumulated sand downwind a low rise house in Waldport, Oregon. The flow topology depicted in Fig. 5(m) is confirmed

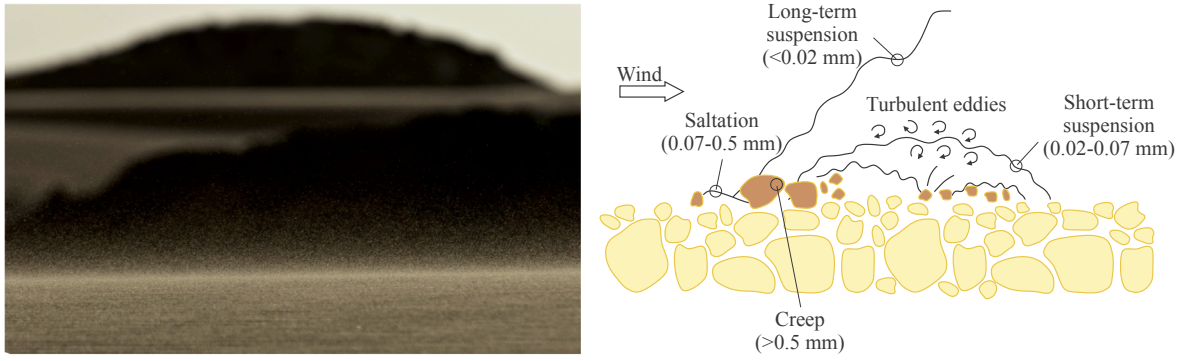

Fig. 4. Sand grains during saltation (a, explicit publishing permission from the owner of the photo: Nik Barte, www.nikbarte.it), windblown sand transport modes of motion (b, redrawn from [50]).

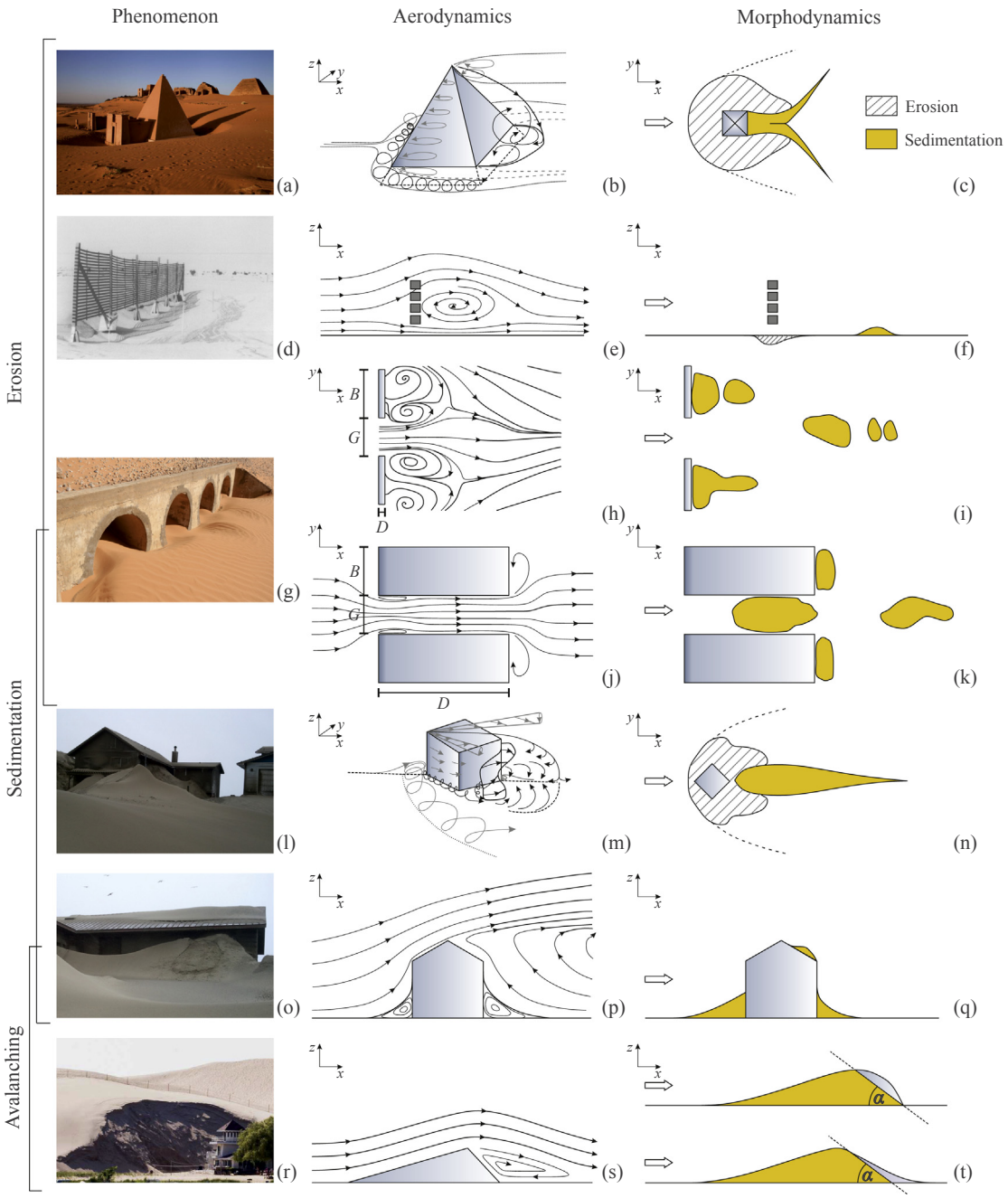

Fig. 5. Windblown sand around built structures. Scour effect around a Meroe Pyramid in Sudan (a, explicit publishing permission from the owner of the photo: Boris Kester, www.traveladventures.org), 3D flow pattern around a pyramidal obstacle (b, redrawn from [58]), sand erosion pattern (c, redrawn from [59]). Venturi effect under a porous sand fence (d, reprinted from [60], with the permission from the Geological Society of London), wind flow mean streamlines (e), eroded and sedimented sand (f). Partial obstruction of embankment culverts (g), $D \ll B$: time-averaged streamlines between two solid barriers (h, redrawn from [61]), sand accumulation zones (i, redrawn from [62]); $D > B$: time-averaged streamlines in a conduct (j), sand accumulation zones (k). Shadow dune in the lee of a house in Waldport, Oregon (l, explicit publishing permission from the owner of the photo: Jason Durrett), qualitative flow around a cube with 45° incidence angle (m, redrawn from [63]), sand sedimentation pattern (n, redrawn from [59]). Sand accumulation on a gable roof in Waldport, Oregon (o, explicit publishing permission from the owner of the photo: Jason Durrett), flow pattern around a building with 30° roof pitch (p, redrawn from [64]), sand sedimentation pattern (q). Sand avalanching from a migrating dune at the Silver Lake, Michigan (r, explicit publishing permission from the owner of the photo: Andraya Croft), flow around an ideal transverse dune (s), dune shape before and after avalanche (t).

by a number of wind tunnel tests around surface-mounted finite-height prisms at various incidences, from [56] to [63]. The near wake topology is characterized by a closed arch-vortex, that entrains the surrounding fluid from both sides and from the top towards the axis of symmetry of the wake. In such a way, the sedimented sand shapes as an elongated, alongwind symmetric, and narrow dune (Fig. 5n, also called “sand shadow” in geomorphology literature). Such kinds of sand shadow have been reported in the geomorphology literature for a variety of natural obstacles, e.g. in the lee of small boulders and bushes but also mountains (e.g. [53,69]).

Fig. 5(o) shows sand accumulated on the downwind pitch of a gable roof. According to the flow pattern in Fig. 5(p) the flow separates along the ridge and does not reattach onto the roof [64]. The local low-speed wind in the reversed flow regions promotes sand sedimentation on the

roof right downwind the ridge, other than around the upwind and downwind vertical walls of the building (Fig. 5q).

Sand *avalanching* re-shapes the accumulated sand, where the accumulation profile locally exceeds the sand natural angle of repose. The angle of repose for medium-fine sands is typically $\alpha = 32–34°$ [53]. Sand avalanches can take place at different scales. In Fig. 5(o) a small avalanche comes down from a steep accumulation profile downwind a house. In Fig. 5(r) a dozen meter-long sand avalanche develops along the whole downwind face of a large migrating dune. The flow around a transverse dune is schematically depicted in Fig. 5(r): the boundary layer separates at the dune crest, and an elongated reversed flow region takes place downwind it (Fig. 5s). The sand sedimentation rate is very high just downwind the crest, and deceases towards the dune downwind toe. Recurrent avalanches slide down from a line close downwind the crest (also called “brick” line, in geomorphology literature, Fig. 5t).

3. Windblown Sand Limit States

We define windblown Sand Limit States (SLSs) as threshold performance levels beyond which the structure or the infrastructure no longer fulfills its design criteria under sand action. SLSs are classified into Sand Ultimate Limit States (SULSs) and Sand Serviceability Limit States (SSLSs), analogously to safety formats widespread in structural engineering [42]. In general, we define SULSs as the threshold performance level beyond which structure/infrastructure is no longer safe, while attaining SSLSs implies its loss of functionality. SLSs may be specified separately for structures and infrastructures, since windblown sand action is strictly bound to them. In the case of civil structures, SLSs account for both direct and indirect windblown sand action. Attaining SULS involves structural failure, while attaining SSLS involves structural durability issues, service requirements no longer met, and human discomfort. Conversely, in the case of civil infrastructure, SLSs mainly account for indirect windblown sand action and strongly depend on the affected component. Attaining SULS involves service interruption and/or users unsafe conditions, while attaining SSLS involves infrastructure partial loss of capacity and/or users discomfort. In the following, attainable SLSs are briefly discussed by referring to generic structures and infrastructures. SLSs for railways have already been reviewed in [25]. Here, only some noteworthy examples are given for the sake of brevity.

3.1. Sand Ultimate Limit States

SULSs are mainly induced by accumulated sand volume. This schematically occurs under two different environmental conditions. First, when migrating dunes, e.g. barchan ones, encroach a built structure. Secondly, when the structure is near or in a sandy plane. In this case, the structure acts as an obstacle to the incoming sand drift and induces sand sedimentation around it. In both cases, the attainment of SULS causes structural failure. For instance, Fig. 6(a) shows a coastal dune encroaching a house: the active lateral sand pressure induces the collapse of the structure.

Railways SULSs are mainly induced by civil works, when the railway embankment or cutting are buried by sedimented sand. For instance, a desert dune encroaching a railway embankment is shown in Fig. 6(b).

Once civil works attains SULS, the track superstructure attains SULS in turn. For instance, the sedimented sand may jam railroad switches, analogously to snow and ice accretion in cold environments (Fig. 6c). The full or partial covering of a railway segment, or of a component can finally induce the SULS of rolling stock, i.e. running train derailment [70] (Fig. 6d), if train traffic is not suspended as a precautionary measure.

3.2. Sand Serviceability Limit States

Fig. 7 collects some iconic examples of SSLS. Windblown sand encroaching the Algerian town of In-Salah is shown in Fig. 7(a). According to [28], dozens of buildings including houses, schools and administrative buildings were completely and permanently abandoned due to serviceability issues induced by encroaching sand. The sand accumulates not only against buildings facades (Fig. 7b) but also enters indoor spaces (Fig. 7c) obstructing the use of the building. Two remarkable examples of attained SSLS in coastal regions are Bayshore district in Oregon and Shoyna village in Russia. In Bayshore district, houses are built along the backside of a foredune. Because of the strong winds, sand frequently and regularly buries them [71] (see Fig. 5l and o). Shoyna village was settled in the 1930s. Sand dunes started migrating by the action of westerly wind from the 1950s. Nowadays, more than half of the village is buried under sand and population decreased accordingly [72].

Structures built in windblown sand-prone zones can be also subject to windblown sand induced wear. The wear induced by sand on common construction materials in desert environment, such as concrete and adobe blocks, has been investigated by [73–75].

Given the large number of railway infrastructure components, there are many railway SSLSs. Under SSLSs, windblown sand affects only a single component of the railway. However, this can reverberate on the overall railway system performances, i.e. its speed [76]. The sole SSLS attained by civil works is the partial obstruction of embankment culverts by sedimented sand (Fig. 7d). Among track superstructure SSLSs, ballast contamination is the most common one (Fig. 7e). It is generally quantified by referring to an upper permitted level, quantitatively expressed by the Percentage Void Contamination. In particular, an allowable limit of Percentage Void Contamination is set to 30% for a concrete sleeper track with a 250 mm thick ballast layer [77]. Ballast contamination leads in turn to a series of side effects identifiable as SSLSs, e.g. increasing of the stiffness of ballast bed, decreasing of the damping of ballast bed and rail support modulus [78], accumulation of permanent deformation, rail corrugation (Fig. 7f). Sedimented windblown sand can induce abrasive wear inside switches components, rail grinding [79], and wheel profiling of rolling stock (Fig. 7g).

(a) (b) (c) (d)

Fig. 6. Windblown Sand Ultimate Limit States. House collapse due to active lateral sand pressure from an encroaching sand dune at the Silver Lake in Michigan, (a, before and after the attainment of the SULS), full sand coverage of a railway due to encroaching sand dune in Namibia (b, explicit publishing permission from the owner of the photo: Giles Wiggs), railroad switch jammed by sedimented sand in Algeria (c), train derailment in Namibia (d, reprinted from [34] with the permission from the editor).

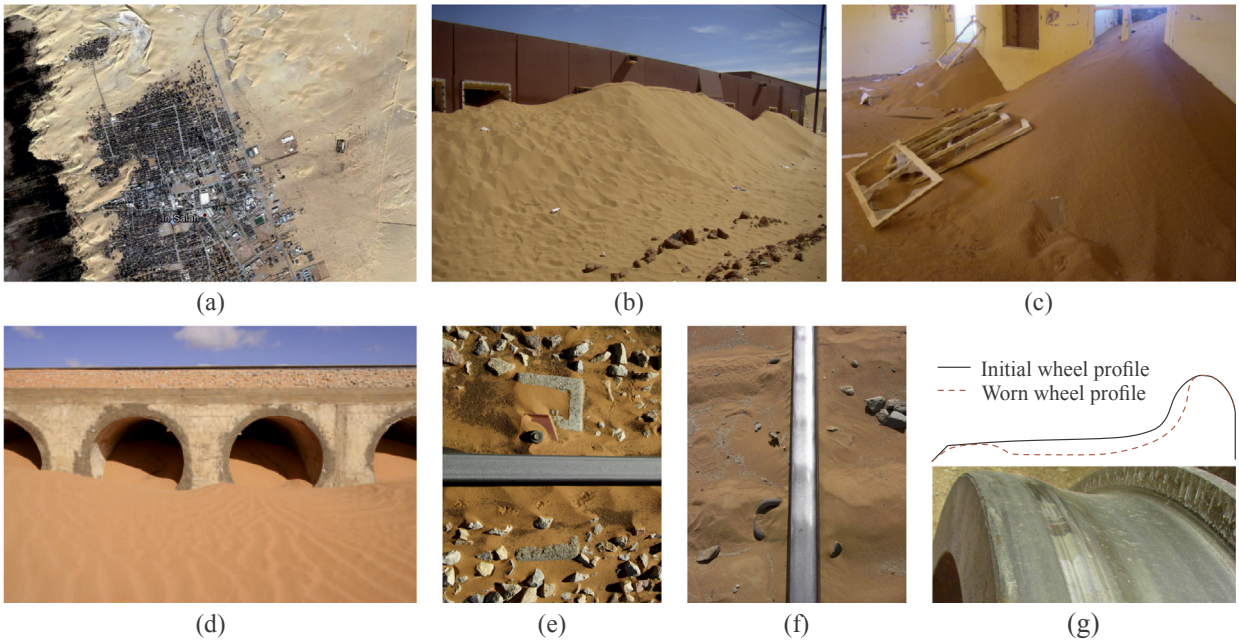

Fig. 7. Windblown Sand Serviceability Limit States. Sand encroaching In-Salah, Algeria (a, from Google Earth year 2002), sand sedimented against a single building in In-Salah (b, explicit publishing permission from the owner of the photo: Nouar Boulghobra), indoor sand infiltration in In-Salah (c, reprinted by permission from RightsLink: Springer [40], owner of the photo: Nouar Boulghobra). Partial obstruction of embankment culverts in Algeria (d), ballast contamination in Algeria (e), rail corrugation in Jordan (f, reprinted by permission from RightsLink: Springer [80]), wheel profiling in Saudi Arabia (g, reprinted from [81]).

4. Modelling of windblown sand action

In the following, we propose a framework for the definition and probabilistic quantification of the windblown sand as an environmental variable action. The metric describing windblown sand action can vary depending on the SLS. However, for most SLSs, the local windblown sand action can be directly related to the volume of sedimented sand around the generic structure.

4.1. Modelling of incoming sand transport rate

We define the incoming windblown sand transport rate Q_{in} as the mean volume per crosswind meter per hour of sand carried by the incoming wind undisturbed by specific obstacles, in analogy to the incoming mean wind velocity in wind engineering practice ([7], Sect. 4). Q_{in} rigorously follows from the integral of the windblown sand saltation flux profile $q(z)$ along the vertical direction z (Fig. 8). Practically, Q_{in} is usually modeled by means of semi-empirical expressions [51], that heuristically account for the features of both the wind and the sand bed. Q_{in} is subject to the equilibrium condition $\tau > \tau_t$, where τ is the wind-induced shear stress at the sand bed surface, and τ_t is the sand bed resistance to saltation, i.e. the lower value of the shear stress at which sand grains loose their static equilibrium (Fig. 8). τ is usually replaced by the so-called wind shear velocity as $u_* = \sqrt{\tau/\rho}$, where ρ is the air density. In turn, u_* is recovered from the mean wind speed velocity profile in atmospheric boundary layer for a given aerodynamic roughness length z_0 as $u_* = 0.41 U_{ref}/\ln(z_{ref}/z_0)$. Usually, the reference height is adopted as $z_{ref} = 10$ m, and the corresponding wind speed U_{10} is averaged over 10 min, i.e. the effect of the wind turbulence fluctuations on Q_{in} is neglected. Moreover, it is worth stressing that Q_{in} is estimated by considering neutral atmospheric conditions, flat orography and absence of obstacles. These features represent, however, standard conditions for desert environments. Analogously, τ_t is replaced by the so-called threshold shear velocity u_{*t}, usually expressed by deterministic empirical functions of the sand grain mean diameter d [52]. In this study, u_{*t} refers to dry, loose, bare sand and ignores environmental effects, such as soil moisture, salt concentration and sand crusting. Indeed, a statistical description of such environmental effects on u_{*t} is not practically feasible since they dramatically vary in both space and time. Nevertheless, they can be taken into account a posteriori through the adoption of environmental factors in a semi-probabilistic framework. It follows that all the semi-empirical expressions of windblown sand transport rate take the form $Q_{in} = Q_{in}(u_*, u_{*t})$.

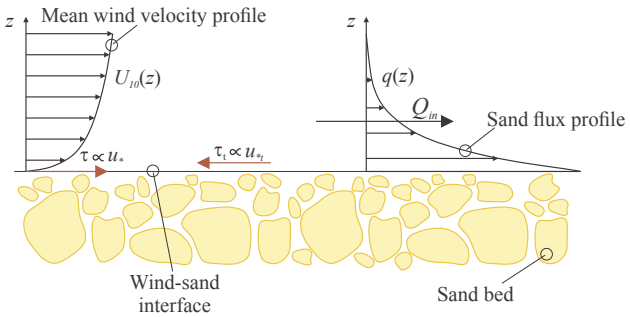

Fig. 8. Wind velocity and sand flux profiles during saltation.

It is worth stressing that u_* and u_{*t} are bulk random variables that incorporate the effects of natural phenomena varying in both space and time. However, Q_{in} models are deterministic and account for the wind speed variability in mean terms only and do not account for threshold shear velocity variability at all. We recently discussed u_{*t} variability in [82,83]. We provided a fully probabilistic modelling of Q_{in} in [49], where u_{*t} is described by non-parametric kernel distributions, while u_* is described by the Hybrid-Weibull distribution. In the light of this, Q_{in} is expressed via the model by [84], here reported in probabilistic terms:

$$f(Q_{in}) = C\sqrt{\frac{d}{d_r}}\frac{\rho}{g} f(u_*)^3 \left[1 - \frac{f(u_{*t}\,|\,d)}{f(u_*)}\right] \quad \text{if } u_* > u_{*t}$$
$$f(Q_{in}) = 0 \quad \text{if } u_* \leqslant u_{*t} \tag{1}$$

where $C = 6.7$ is an empirical constant, $d_r = 0.25$ mm is the reference grain diameter, g is the acceleration of gravity, and $f(\cdot)$ stands for Probability Density Function (PDF).

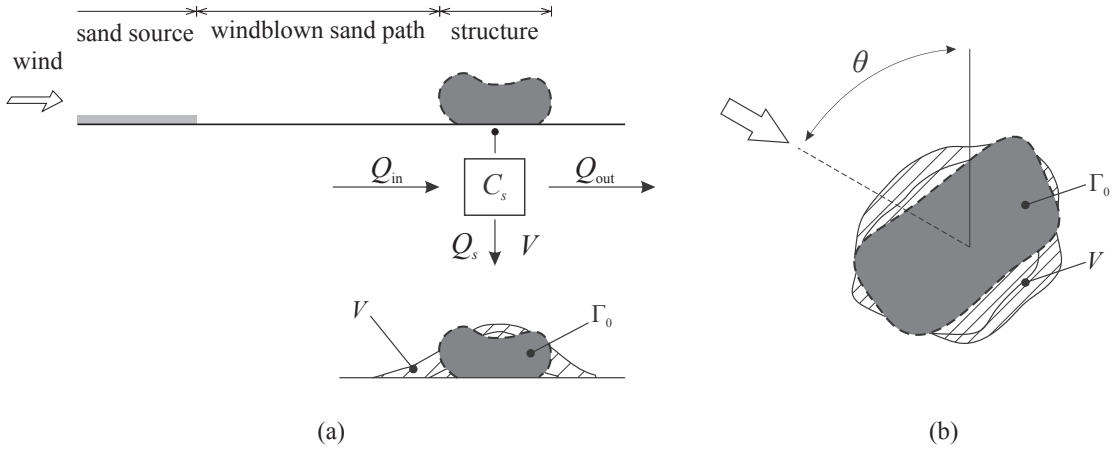

Fig. 9. Sand action conceptual scheme (a) and dependance with respect to wind yaw angle θ (b).

4.2. Modelling of local windblown sand action

Fig. 9(a) shows the modelling scheme and related state variables of the local windblown sand action on a general structure. Under unsteady state conditions, the incoming sand transport rate Q_{in} splits into the sedimentation rate Q_s and the outgoing (i.e. filtered) transport rate Q_{out}. We define the local sand action around the generic structure as the accumulated sand volume V. V results from the time-cumulated sedimentation rate Q_s, that is related to the incoming windblown sand Q_{in} by the sedimentation coefficient C_s. C_s is defined as the ratio between Q_s and Q_{in}. In general, C_s depends on both the incoming sand transport rate yaw angle θ and the overall shape of the specific obstacle Γ analogously to the force coefficients for the wind action ([7], Sect. 7). However, it is worth stressing a substantial difference: the overall shape of the obstacle Γ is now described by a virtual geometry that varies over time and depends on the initial geometry of the structure Γ_0 and on V. Hence, we can write $C_s = C_s(\theta, \Gamma_0, V)$. It is worth stressing that C_s referred to path SMMs translates into their sand trapping efficiency (see Section 1). As a result, high values of C_s are preferred for such design solutions, i.e. most of the sand is trapped by the path SMM. Conversely, low values of C_s are preferred for generic structures. This implies that most of the sand overtakes the structure and less sand sediments around it.

Given the lack of a closed form for C_s, its semi-empirical expression can be obtained from wind tunnel tests and/or computational simulations. For fixed θ and Γ_0, Q_{out} is expected to increase with increasing accumulated sand volume while Q_{in} tends to zero. It follows that $C_s(V)$ has a monotonic decreasing trend and $C_s \in [0, 1]$. In probabilistic modelling terms, Q_s and Q_{out} can therefore be obtained as PDFs as follows

$$f(Q_s) = C_s(\theta, \Gamma_0, V) f(Q_{in}) \tag{2}$$

$$f(Q_{out}) = [1 - C_s(\theta, \Gamma_0, V)] f(Q_{in}) \tag{3}$$

The windblown sand action is then modeled as a random variable because of the large uncertainty involved in the phenomenon. The PDF of the total volume accumulated over a time period t can be obtained as the mixture of convolutions:

$$g\Big(V(t)\Big) = \sum_{n=1}^{\infty} (f_1 * f_i * \ldots * f_n) Q_s \mathrm{P}[N_\theta = n] \tag{4}$$

where $f_i = f$ for $i = 1, \ldots, N_\theta$, and N_θ is the number of occurrences in which the wind blows from the direction θ over t.

In order to assess the structure performance, V must be referred to the structure resistance. For most SLSs, it can be expressed as a resistant sand volume V_R. The attainment of V_R implies structure/infrastructure failure, e.g. the overturning of a wall for lateral sand pressure or the full coverage of the railway track superstructure, or alternatively SMM failure, i.e. too low SMM efficiency. For a generic structure/infrastructure, V_R can be defined according to a chosen SLS, while for a given path SMM, V_R can be defined as the SMM nominal capacity $\overline{V}$, i.e. the maximum volume of sand that can be trapped, or better as a ratio of $\overline{V}$. In any case, sand maintenance removal is required before V_R is reached. It is worth stressing that the definition of structure/infrastructure resistance through the bulk quantity V_R alone is not suitable when the windblown sand action is assessed on a localized component, e.g. a railroad switch. In such cases, the shape of sedimented sand profile plays a major role since the resistance is better quantified by the local thickness of the sand accumulated on the component.

Given the time-variant sand action $V(t)$, a time-variant reliability analysis is required in order to assess the characteristic time of failure of a generic structure subject to windblown sand action. The basic condition for a satisfactory state in a reliability analysis framework can be defined as [85]:

$$V(t) < V_R(t) \tag{5}$$

The probability of exceedence $p_f(t)$ of the sand action with respect to the resistant volume is equal to:

$$p_f(t) = P[V(t) \geqslant V_R(t)] = \int_0^{+\infty} F_{V_R}\Big(x, t\Big) f_V\Big(x, t\Big)\, dx \tag{6}$$

where F_{V_R} is the Cumulative Distribution Function (CDF) of V_R. In general, V_R is time-constant and can be described by its nominal value whatever the nature of the structure is, since its degree of uncertainty is much lower than the one of V. Hence, Eq. (6) becomes:

$$p_f(t) = P[V(t) \geqslant V_R] = 1 - F_V(V_R, t) \tag{7}$$

where F_V is the CDF of V. The characteristic time of failure T_k can be defined as the time during which the condition (5) is violated only with a given probability $p_{f,k}$, i.e. $p_f(T_k) = p_{f,k}$. Assuming the monotonous function $V(t)$, p_f is also monotonous and its inverse function can be defined. Hence, the characteristic time of failure can be derived as

$$T_k = p_f^{-1}(p_{f,k}) \tag{8}$$

In summary, Fig. 10 shows a generic trend of the time-variant sand action through its PDF $f_V(t)$, the mean value $\mu_V(t)$, and the increasing trend of $p_f(t)$.

5. Application and results

The proposed modelling framework is beyond the current state of the art reviewed in Section 1. The lack of long term and detailed in situ measurements does not allow proper validation. Very scarce laboratory measurements only partially allow the quantification of the

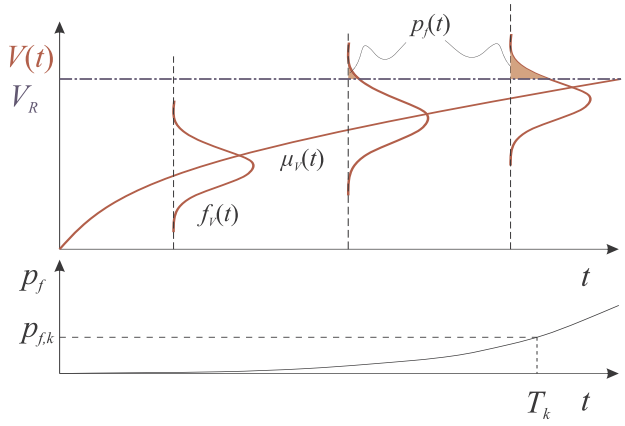

Fig. 10. Time-variant sand action and related probability of failure.

sedimentation coefficient. Nevertheless, in the following an effort is accomplished to put the framework at work aimed at demonstrating the technical feasibility of the approach in an engineering design perspective. The proposed application refers to a desert railway infrastructure protected by two alternative design solutions. The study layout is outlined in Section 5.1, while the obtained results are discussed in Section 5.2.

5.1. Study layout

The selected site is located in the Arabian peninsula near the Hafr-al-Batin city, along the 2750 km long North-South Railway line linking Al-Haditha and Jalamid with the new port city Ras Al-Khair (Fig. 11a). The railway alignment around the site develops along the West-East direction, and it crosses the sand migration prevailing path from the An-Nafud desert to the Rub-al-Khali sand sea through the Ad-Dahna corridor. It follows that Q_{in} mainly attacks the railway from the North side and South side. The sand consists of medium sized, well sorted quartz grains. The mean sand grain diameter is set equal to $d = 0.35$ mm [86]. The aerodynamic roughness z_0 is set equal to $z_0 = 4e{-}3$ m, a common value for sandy desert terrains. The wind speed dataset refers to the 10-min average wind velocity U_{10} recorded by an anemometric station from Jan 2007 to Dec 2012 with a time sampling $\Delta t = 1$ hr. The wind speed is measured over 36 directions with sampling yaw angle $\Delta\theta = 10°$.

The available dataset includes some missing data due to malfunctions or operational problems of the anemometric station. Missing data are estimated equal to 9% and are evaluated to be almost uniformly distributed along the hours of the day. Both time sampling and missing data are sources of incompleteness of the dataset. In the literature, randomly distributed data incompleteness is recognised as not influential on the probability distribution of U_{10}, while it may lead to underestimations of the extreme values [87].

Fig. 11(b) shows the modelling framework and the related state variables for a single side of the railway corridor. Such a scheme results directly from the general one in Fig. 9, by putting in series three objects, each of them inducing a local windblown sand action, i.e. V_1 acting on the SMM, V_2 acting on the embankment, and V_3 acting on the track superstructure. The same mirrored scheme holds for the opposite side of the railway. The setup geometries are shown in Fig. 11(c and d). Two types of path SMMs are alternatively tested: a common Straight Vertical Wall (SVW) [47], and the Shied for Sand (S4S) aerodynamically shaped barrier [44]. They are both solid barriers that aim at inducing sand sedimentation upwind the SMM by generating a stable upwind vortex that lowers the local shear stress below the threshold (see Eq. (1)). The height of the SMMs and of the embankment are set equal to 4 m and 2.5 m, respectively. A double-track railway is considered, with a 0.25 m width ballast bed.

The sedimentation coefficients C_s of both SMMs, the embankment, and the track superstructure are plotted as a function of the dimensionless sand action $V/\overline{V}$ for $\theta = 90°$ in Fig. 12. The experimental values of C_s referred to a basic SVW and a generic embankment are derived from the wind tunnel tests made by Hotta and Horikawa [88]. Conversely, the values of C_s referred to S4S have been directly obtained by the authors in the framework of a wind tunnel test intended for the estimation of its efficiency for increasing V [44]. Hence, the experimental data is fitted with continuous monotonic decreasing functions that exhibit $C_s(V/\overline{V} = 1) = 0$, i.e. null Q_s and maximum Q_f when the nominal capacity is reached. To our best knowledge, the only studies that provide time-varying V, and therefore C_s, are [88,44], but only for $\theta = 90°$. Unfortunately, the literature particularly lacks of studies addressed to track superstructure induced sand morphodynamics. Therefore, $C_{s,3}$ is purely conjectured constant up to the filling of ballast voids (i.e. Percentage Void Contamination equal to 100%), and then linearly decreasing up to $V = \overline{V}$. As such, we conjecture that first the sand fills the ballast voids, and then it accumulates uniformly on the surface of the railway superstructure.

During the lifetime of the infrastructure, the sand sedimented around any SMMs, embankment, and track superstructure need to be periodically removed in order to avoid failure. In this study, V_R is set on the basis of a performance-based criterion. The SMMs V_R is defined as the sand volume that induces a decrease of the efficiency equal to 20% the initial value, i.e. $C_{s,1}(V_R/\overline{V}) = 0.8C_{s,1}(V/\overline{V} = 0)$. The embankment V_R is set as the sand volume that induces a decrease of $C_{s,2}$ equal to 50% the initial value, i.e. $C_{s,2}(V_R/\overline{V}) = 0.5C_{s,2}(V/\overline{V} = 0)$. The results discussed in the following refer to the attainment of SULS for full covering of the track superstructure. As a result, the track superstructure V_R is set equal

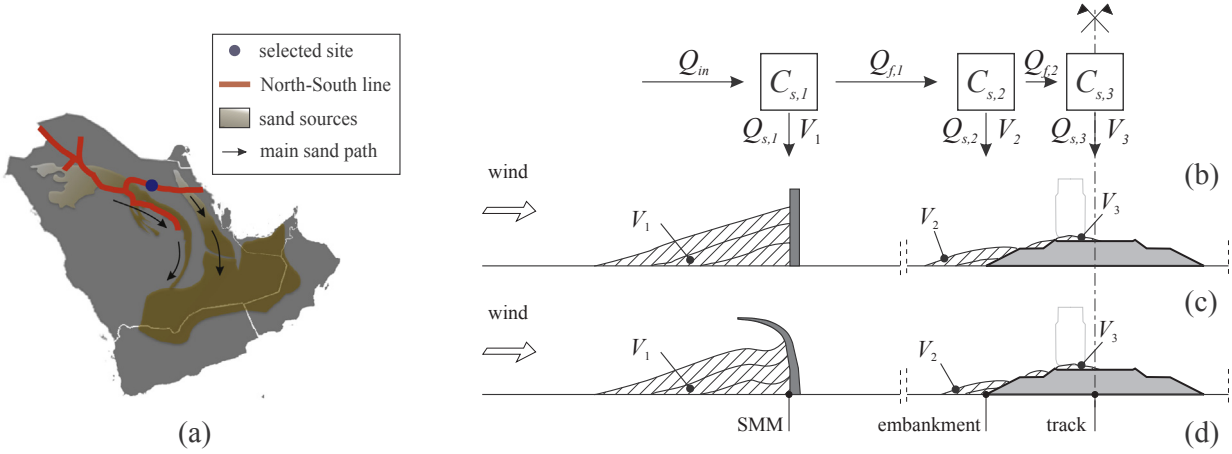

Fig. 11. Selected site (a), modelling framework and related state variables (b), scheme of the setup geometry with SVW (c) and with S4S (d) as SMM for increasing V.

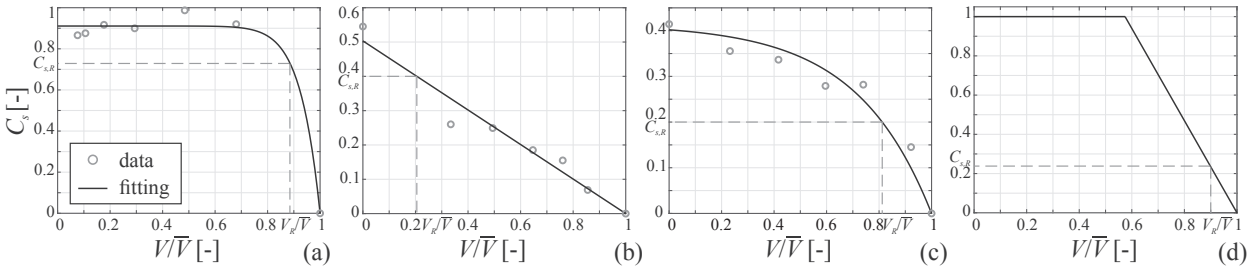

Fig. 12. Sedimentation coefficients versus $V/\overline{V}$: Shield for Sand (a), Straight Vertical Wall (b), embankment shoulder (c), track superstructure (d).

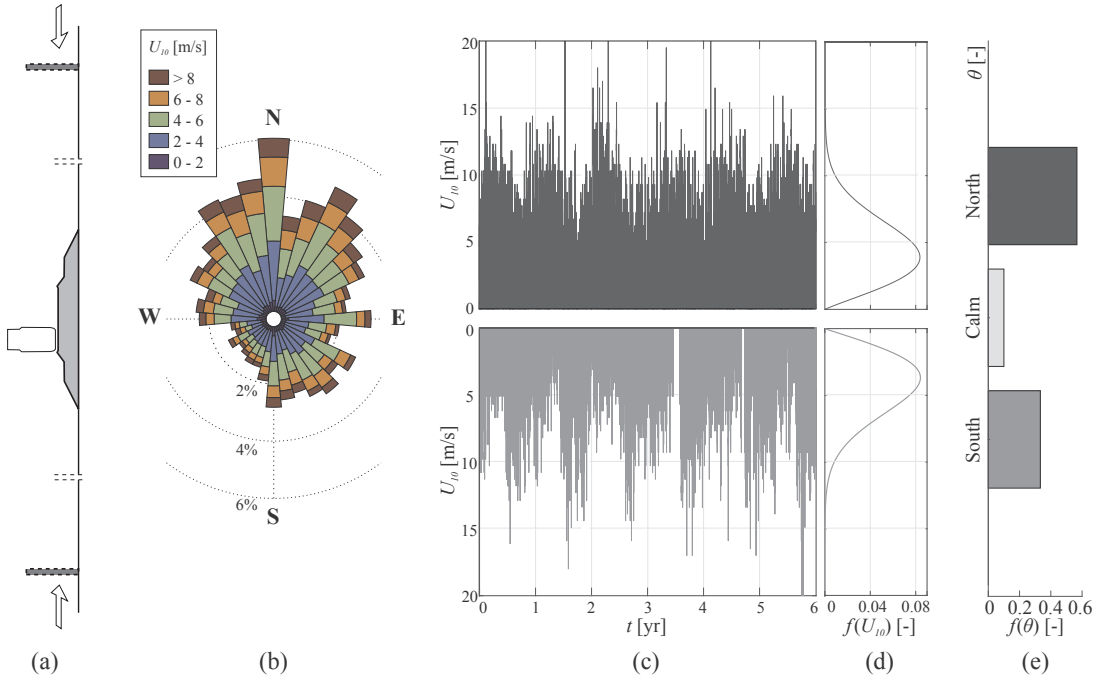

Fig. 13. Incoming wind statistics. Geometrical setup (a), wind rose (b), North and South U_{10} time series (c), probability density functions (d), North and South direction occurrences (e).

to $V_R = 0.9\overline{V}$. The dimensionless resistant volume $V_R/\overline{V}$ and the correspondent sedimentation coefficient $C_{s,R}$ are drawn as dashed lines in Fig. 12.

In order to assess the non-linear model outlined by Eqs. (2)–(4), a Monte Carlo simulation based on bootstrapping technique is performed on the basis of $f(U_{10})$ and $f(u_{*t})$. $f(U_{10})$ is derived from the wind speed dataset. $f(u_{*t})$ is obtained directly from [82]. Q_{in} is modeled as a stationary, non-Gaussian random process. As a result, Q_{in} is decomposed into a series of independent incoming sand transport rates. The low-frequency, high-amplitude cycles related to macro-meteorological fluctuations of the wind speed, i.e. time-correlations at the annual, synoptic, and diurnal time scales, are discarded. In light of these remarks, and bearing in mind the cumulative nature of V, windblown sand action recalls somehow wind-induced fatigue loading by means of the "state approach" commonly adopted in the practice [89,49]. The Monte Carlo simulation accounts for about 22e + 6 realizations for each specific obstacle under both SMM setups. The probability of failure is set equal to $p_{f,k} = 5\%$ so that failure is defined with respect to the characteristic value of the sand action V_k, i.e. its 95th percentile $p_{95}(V)$.

5.2. Results

The incoming sand transport rate is assumed in the worst case scenario, i.e. perpendicular to the obstacle, by analogy with common wind engineering practice. As a result, Q_{in} derives from the side-PDFs of the incoming wind speed, i.e. the non-directional PDFs of U_{10} blowing from North and South sides of the railway. Wind statistics are collected in Fig. 13. The wind rose recalls a obtuse bimodal regime (Fig. 13b). Time series of the Northerly and Southerly recorded wind speed are plotted in Fig. 13(b) and condensed in Fig. 13(d) as classic Weibull PDFs. Finally, Fig. 13(e) plots the discrete distribution of the wind direction θ categorized as North, South and Calm. It is worth highlighting that, although northerly winds are more common, the North and South $f(U_{10})$ are tantamount.

Fig. 14 collects the main results derived from windblown sand action modelling framework with incoming sand transport rate from the North side of the railway and SVW setup. Fig. 14(a–c) plots a 1-year long realization of the incoming (Q_{in}) and filtered ($Q_{f,1}$, $Q_{f,2}$) sand transport rate versus time t in order to show the model workflow. The filtering effect on the sand transport rate is clearly depicted by the fall of its magnitude each time an obstacle is overcome. Fig. 14(d–f) collects the realizations of the windblown sand action V and related statistics, i.e. mean values μ and i-th percentiles p_i, versus time. It is worth highlighting that while V_1 and V_2 directly result from northerly Q_{in}, V_3 results from both northerly and southerly Q_{in}. Discarding the macro-meteorological features of the wind velocity helps us distinguish the effect of the trend of C_s on the evolution of V. The general trend of V is nonlinear monotonic increasing and tends to a horizontal asymptote defined by the obstacle nominal capacity $\overline{V}$. Indeed, the monotonic decreasing trend of C_s induces a monotonic decreasing gradient of V up

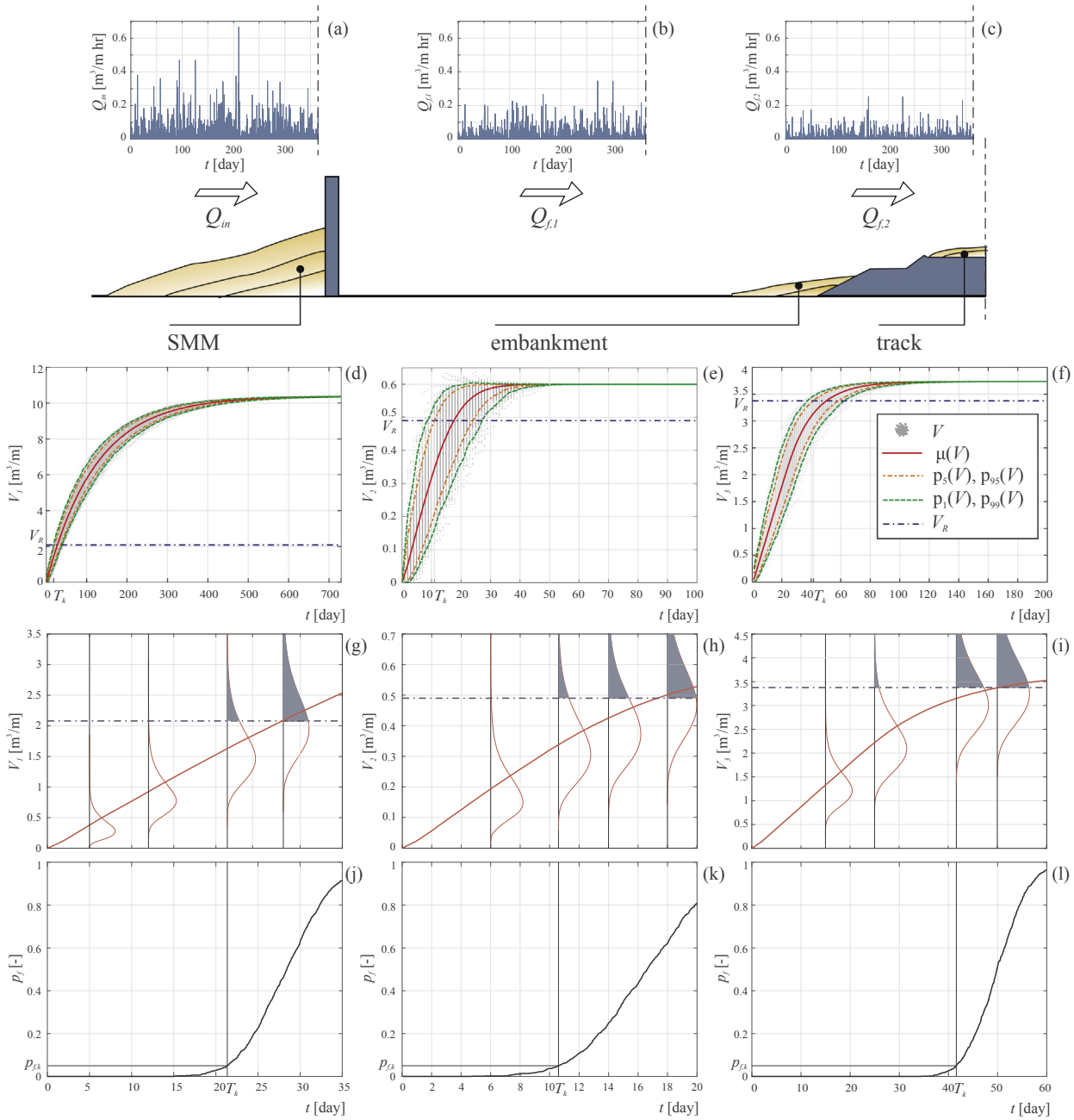

Fig. 14. North side of the SVW railway setup. Incoming sand transport rate (a), sand transport rate filtered by SVW (b), sand transport rate filtered by the embankment (c). Windblown sand action on SVW (d), embankment (e), track superstructure (f). Close up view of the windblown sand action in the interest time-period on SVW (g), embankment (h), track superstructure (i). Probability of failure referred to SVW (j), embankment (k), track superstructure (l).

to zero. Once V reaches $\overline{V}$, the equilibrium condition reflected by the null value of C_s does not allow the sand to accumulate anymore. Furthermore, the randomness of V initially increases and then diminishes approaching $\overline{V}$. Fig. 14(g–i) provides a close-up view of $f(V)$ in proximity to the characteristic time of failure T_k while Fig. 14(j–l) plots the related growing probability of failure p_f. Generally, $f(V)$ are non-Gaussian with time-varying skewness from positive to negative values. Failure is reached in chronological order on the embankment, on the SVW and finally on the track.

Fig. 15 collects the characteristic times of failure for the SMMs T_{k1}, the embankment T_{k2}, and the track superstructure T_{k3} resulting from the adoption of SVW or S4S along both North and South railway sides. For a given SMM, the higher the side incoming wind occurrence (Fig. 13e), the lower the characteristic time of failure. For both sides, the S4S barrier performs better than SVW in terms of higher T_k because of its higher nominal capacity and sedimentation coefficient. This result is supported by the purely aerodynamic study performed on both solid barriers by [47] in terms of sand accumulation potentials. The obtained characteristic times of failure does not account for macro-meteorological effects. As a result, they can be rather interpreted as average characteristic times of failure. The time-scales of T_k can help establish if the contribution of long-term large-amplitude cycles related to macro-meteorological fluctuations of the mean wind speed can be relevant. Indeed, while the SVW setup can be mainly sensitive to diurnal and synoptic time-scales, the S4S setup can also be sensitive to larger time-scales, i.e. seasonal and annual ones.

6. Conclusions and perspectives

Windblown sand action and its effect on civil structures remain for

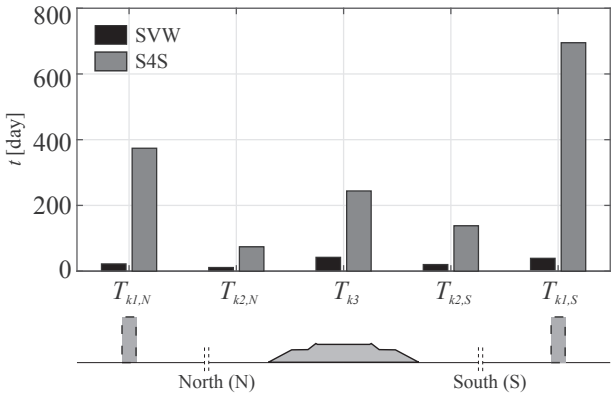

Fig. 15. Characteristic times of failure related to SVW and S4S design solutions.

the time being overlooked in structural engineering despite the broad spectrum of windblown sand induced issues reviewed in this paper. The present study aims at reducing the existing gaps by introducing the definition of, and by proposing a modelling framework for windblown sand action on civil structures. Windblown sand is defined as an environmental variable action by analogy with wind and snow drift actions, commonly taken into account in structural engineering. Windblown sand action is accounted for via the accumulated sand volume around the affected structure. Such a sand volume translates into both direct static loads on structural elements and indirect actions that undermine durability, the performance of the structure, human comfort, human safety conditions, and give rise to maintenance operations. The effects of windblown sand action on civil structures and infrastructures are categorized into Sand Ultimate Limit States and Sand Serviceability Limit States, bearing in mind the common design criteria in structural engineering. The proposed probabilistic model involves the assessment of the incoming sand transport rate to the affected structure and the local windblown sand action on it. The reliability of a specific structure can then be ascertained by means of a time-variant reliability analysis. Having in mind the needs in structural engineering, the technical applicability of the proposed framework has been demonstrated by referring to a desert railway infrastructure protected by two alternative design solutions against windblown sand action. From the obtained results, some general comments can be draw in a design perspective. First, the model allows to quantify the performances of alternative design solutions and to select the best option. In this case, Shield for Sand increases considerably the time of failure up to two years, and it will in turn lower sand removal costs. Secondly, the higher the wind occurrence, the lower the sand removal period, for a given SMM capacity. Conversely, for a chosen sand removal period, the higher the wind occurrence, the higher the required capacity to be met by properly sizing the SMM. In summary, the obtained results allow to assess the characteristic values of the windblown sand action, the performances of the sand mitigation measures and plan sand removal maintenance operations.

In the light of this newborn, wide research field, we suggest the following research perspectives to the whole scientific community in order to fill the gaps of knowledge emerged by the present study. First, we strongly encourage further experimental studies addressing the assessment of the sand sedimentation pattern, and the sedimentation coefficients in turn, around multiple structure geometries under different environmental setups, e.g. incoming sand transport rate yaw angle, and diverse wind flow features, such as Reynolds number. Secondly, macro-meteorological broadband random component together with annual, synoptic, diurnal cycles of the wind speed can be incorporated into the modelling of the incoming sand transport rate. This can be done by simulating synthetic mean wind speed time series by adopting both its fitted probability density function and the wind power spectrum associated with the macro-meteorological peak [90]. Thirdly, in a limit state design perspective, a semi-probabilistic approach to windblown sand action can be derived from the same proposed fully probabilistic approach. First, the partial safety factor γ can be derived a posteriori as $\gamma = V_d/V_k$, being V_k and V_d the characteristic and the design values of the sand action corresponding to a target very low probability of failure. Second, the effects of uncertain, highly variable environmental conditions such as soil moisture, sand salt concentration or sand crusting, could be taken into account by semi-empirical factors.

We hope that future independent studies will be addressed to assess the accuracy of the proposed model by means of experimental campaigns and further develop this contribution in order to achieve a more robust probabilistic framework for the evaluation of windblown sand action on structures.

Acknowledgments

The study has been conceived within the MSCA-ITN-2016-EID research project Sand Mitigation around Railway Tracks (SMaRT, www.smart-eid.eu). The SMaRT project has received funding from the European Union Horizon 2020 research and innovation program under grant agreement No. 721798. The study has been developed in the framework of the Windblown Sand Modelling and Mitigation (WSMM) joint research, development and consulting group established between Politecnico di Torino and Optiflow Company. The authors wish to thank the other members of the WSMM group for the helpful discussions about the topics of the paper. The authors would like to acknowledge the permissions given by various organizations and individuals to reproduce figures for this paper. In particular, we would like to thank Nouar Boulghobra (C.R.S.T.R.A - Algeria), Voestalpine, Nik Barte, and Jason Durrett for the pictures they generously shared with us.

References

[1] Davenport AG. The response of slender line-like structures to gusty wind. In: Preoceedings of the Institution of Civil Engineers, vol. 23; 1962. p. 389–408.
[2] Simiu E, Scanlan RH. Winds effects on structures: fundamentals and applications to design. 3rd ed. New York: Wiley; 1996.
[3] DGII-D3. Scientific Support Activity in the Field of Structural Stability of Civil Engineering Works. Snow Loads - FINAL REPORT, Tech. rep., COMMISSION OF THE EUROPEAN COMMUNITIES; 1998.
[4] O'Rourke M, DeGaetano A, Tokarczyk JD. Analytical simulation of snow drift loading. J Struct Eng 2005;131(4):660–7. https://doi.org/10.1061/(ASCE)0733-9445(2005)131:4(660).
[5] Zhou X, Qiang S, Peng Y, Gu M. Wind tunnel test on responses of a lightweight roof structure under joint action of wind and snow loads. Cold Regions Sci Technol 2016;132:19–32. https://doi.org/10.1016/j.coldregions.2016.09.011.
[6] Demartino C, Koss HH, Georgakis C, Ricciardelli F. Effects of ice accretion on the aerodynamics of bridge cables. J Wind Eng Ind Aerodynam 2015;138:98–119. https://doi.org/10.1016/j.jweia.2014.12.010.
[7] EN 1991-1-4. Eurocode 1: Actions on structures - part 1-4: General actions - wind actions - en 1991-1-4; 2005.
[8] EN 1991-1-3. Eurocode 1: Actions on structures part 1-3 general actions - snow loads - en 1991-1-3; 2002.
[9] Tabler RD. Controlling blowing and drifting snow with snow fences and road design, Tech. rep. National Cooperative Highway Research Program Transportation Research Board of the National Academies; 2003. <https://www.esf.edu/willow/lsf/Litterature/Tabler>.
[10] ISO 12494:2017. Atmospheric icing of structures.
[11] Corti S, Molteni F, Palmer TN. Signature of recent climate change in frequencies of natural atmospheric circulation regimes. Nature 1999;398:799–802. https://doi.org/10.1038/19745.
[12] Giorgi F. Climate change hot-spots. Geophys. Res. Lett. 2006;33:L08707. https://doi.org/10.1029/2006GL025734.
[13] Solari G. Thunderstorm response spectrum technique: theory and applications. Eng Struct 2016;108:28–46. https://doi.org/10.1016/j.engstruct.2015.11.012.
[14] Croce P, Formichi P, Landi F, Marsili F. Climate change: impact on snow loads on structures. Cold Reg Sci Technol 2018. https://doi.org/10.1016/j.coldregions.2017.10.009. [in press].
[15] Anderson R, Hallet B. Sediment transport by wind: toward a general model. Geol Soc Am Bull 1986;97:523–35.
[16] Kind R. Mechanics of aeolian transport of snow and sand. J Wind Eng Ind Aerodynam 1990;36:855–66.
[17] Redding JH, Lord JA. Designing for the effects of windblown sand along the new Jessah-Riyadh-Dammam expressway. Symposium on geotechnical problems in

Saudi Arabia. 1981. p. 363–95.
[18] Stipho AS. Aeolian sand hazards and engineering design for desert regions. Quart J Eng Geol 1992;25:83–92. https://doi.org/10.1144/GSL.QJEG.1992.025.02.02.
[19] Martínez ML, Psuty N, editors. Coastal dunes: ecology and conservation. Berlin, Heidelberg: Springer-Verlag; 2004. doi:10.1007/978-3-540-74002-5.
[20] Fookes PG, Lee EM. Desert environments: landscapes and stratigraphy. Geol Today 2009;25(5):172–80. https://doi.org/10.1111/j.1365-2451.2009.00722.x.
[21] Middleton N, Sternberg T. Climate hazards in drylands: a review. Earth-Sci Rev 2013;126:48–57. https://doi.org/10.1016/j.earscirev.2013.07.008.
[22] Sherman DJ, Nordstrom KF. Hazards of wind-blown sand and coastal sand drifts: a review. J Coastal Res 1994(12):263–75www.jstor.org/stable/25735603.
[23] He W, Huang N, Xu B, Wang W. Numerical simulation of wind-sand movement in the reversed flow region of a sand dune with a bridge built downstream. Eur Phys J E 2018;41:53. https://doi.org/10.1140/epje/i2018-11660-5.
[24] Mestoul D, Bensalem R, Adolphe L. Modeling of urban form against sand accumulation in the city of Gourara in southern Algeria. Energy Proc 2017;122:913–8. https://doi.org/10.1016/j.egypro.2017.07.405.
[25] Bruno L, Horvat M, Raffaele L. Windblown sand along railway infrastructures: a review of challenges and mitigation measures. J Wind Eng Ind Aerodynam 2018;177:340–65. https://doi.org/10.1016/j.jweia.2018.04.021.
[26] Parry H. Massive eighty foot tall sand dunes threaten to swallow up homes on the banks of lake michigan, July 2017. <http://www.dailymail.co.uk/news/article-4719294/Sand-dunes-threaten-swallow-homes-near-Lake-Michigan.html>.
[27] Tresca A, Ruz M, Raison S, Grégoire P. Management of aeolian sand transport on a dike, dunkirk seaport, france. In: Coastal Engineering Proceedings, vol. 33, 2012. <https://icce-ojs-tamu.tdl.org/icce/index.php/icce/article/view/6682>.
[28] Boulghobra N. Climatic data and satellite imagery for assessing the aeolian sand deposit and barchan migration, as a major risk sources in the region of in-salah (central algerian sahara). Arab J Geosci 9(450). https://doi.org/10.1007/s12517-016-2491-x.
[29] Zhang C, Zou X, Cheng H, Yang S, Pan X, Liu Y, Dong G. Engineering measures to control windblown sand in Shiquanhe Town, Tibet. J Wind Eng Ind Aerodynam 2007;95:53–70. https://doi.org/10.1016/j.jweia.2006.05.006.
[30] Liu B, Zhang W, Qu J, Zhang K, Han Q. Controlling windblown sand problems by an artificial gravel surface: A case study over the gobi surface of the Mogao Grottoes. Geomorphology 2011;134(3–4):461–9. https://doi.org/10.1016/j.geomorph.2011.07.028.
[31] Salman A, Howari F, El-Sankary M, Wali A, Saleh M. Environmental impact and natural hazards on Kharga Oasis monumental sites, Western Desert of Egypt. J Afr Earth Sci 2010;58(2):341–53. https://doi.org/10.1016/j.jafrearsci.2010.03.011.
[32] Zakeri JA. Investigation on railway track maintenance in sandy-dry areas, structure and infrastructure engineering: maintenance, management. Life-Cycle Des Perform 2012;8(2):135–40. https://doi.org/10.1080/15732470903384921.
[33] Gazette S. Tracks lost in sand, trains suspended, Saudi Gazette. <http://saudigazette.com.sa/article/48288/Tracks-lost-in-sand-trains-suspended>.
[34] Davel Wallis M. Freight Train Derails, Namib Times. <http://namibtimes.net/freight-train-derails/>.
[35] Cheng J, Jiang F, Xue C, Xin G, Li K, Yang Y. Characteristics of the disastrous wind-sand environment along railways in the Gobi area of Xinjiang, China. Atmos Environ 2015;102:344–54. https://doi.org/10.1016/j.atmosenv.2014.12.018.
[36] Kerr R, Nigra JO. Eolian sand control. Bull Am Assoc Petrol Geol 1952;36(8):1541–73.
[37] Alghamdi AA, Al-Kahtani NS. Sand control measures and sand drift fences. J Perform Construct Facil 2005;19(4):295–9. https://doi.org/10.1061/(ASCE)0887-3828(2005)19:4(295).
[38] Hotta S, Harikai S. State-of-the-art in japan on controlling wind-blown sand on beaches. In: Proceedings of the international conference on coastal engineering, no. 32; 2010.
[39] Page M. Clean-up work underway as winds blow huge piles of sand onto roads and paths in cleethorpes. <https://www.grimsbytelegraph.co.uk/news/clean-up-work-underway-winds-1286702>; 2018.
[40] Boulghobra N, Saifi M, Fattoum L. Sand encroachment in the saharan algeria; the not declared disaster - case study: In-salah region in the tidikelt. Planet@Risk 2015;3(1):72–6<https://planet-risk.org/index.php/pr/article/view/172>.
[41] D.T.R.C 2-4.7. Document technique réglementaire c 2-4.7: Règlement neige & vent (version 2013); 2013.
[42] EN 1990, Eurocode - basis of structural design - en 1990; 2002.
[43] Qu J, Zu R, Zhang K, Fang H. Field observations on the protective effect of semi-buried checkerboard sand barriers. Geomorphology 2007;88(1):193–200. https://doi.org/10.1016/j.geomorph.2006.11.006.
[44] Bruno L, Coste N, Fransos D, Lo Giudice A, Preziosi L, Raffaele L. Shield for sand: an innovative barrier for windblown sand mitigation. Recent Patents Eng 12. https://doi.org/10.2174/1872212112666180309151818.
[45] Sañudo-Fontaneda LA, Castro-Fresno D, Coz-Díaz JJ, Rodriquex-Hernandez J. Classification and comparison of snow fences for the protection of transport infrastructures. J Cold Reg Eng 2011;25(4):162–81. https://doi.org/10.1061/(ASCE)CR.1943-5495.0000031.
[46] Li B, Sherman DJ. Aerodynamics and morphodynamics of sand fences: a review. Aeolian Res 2015;17:33–48. https://doi.org/10.1016/j.aeolia.2014.11.005.
[47] Bruno L, Fransos D, Lo Giudice A. Solid barriers for windblown sand mitigation: aerodynamic behavior and conceptual design guidelines. J Wind Eng Ind Aerodynam 2018;173:79–90. https://doi.org/10.1016/j.jweia.2017.12.005.
[48] Rodrigo JS, van Beeck J, Buchlin JM. Wind engineering in the integrated design of princess Elisabeth Antarctic base. Build Environ 2012;52:1–18. https://doi.org/10.1016/j.buildenv.2011.12.023.
[49] Raffaele L, Bruno L, Fransos D, Pellerey F. Incoming windblown sand drift to civil infrastructures: a probabilistic evaluation. J Wind Eng Ind Aerodynam 2017;166:37–47. https://doi.org/10.1016/j.jweia.2017.04.004.
[50] Pye K. Aeolian dust and dust deposits. Academic Press; 1987.
[51] Kok JF, Parteli EJR, Michaels TI, Karam DB. The physics of wind-blown sand and dust. Rep Prog Phys 2012;75(10):106901. https://doi.org/10.1088/0034-4885/75/10/106901.
[52] Shao Y. Physics and modelling of wind erosion. Springer; 2008. doi: 10.1007/978-1-4020-8895-7.
[53] Pye K, Tsoar H. Aeolian sand and sand dunes. Springer; 2009. doi: 10.1007/978-3-540-85910-9.
[54] Fryberger S, Dean G. A study of global sand seas, Ch. Dune forms and wind regime; 1979. p. 137–55.
[55] Jackson PS. The flow round obstacles in boundary layers Ph.D. thesis University of Cambridge; 1973.
[56] Martinuzzi R, Tropea C. The flow around surface-mounted, prismatic obstacles placed in fully developed channel flow. J Fluids Eng 1993;115:85–92. https://doi.org/10.1115/1.2910118.
[57] Mayaud JR, Webb NP. Vegetation in drylands: effects on wind flow and aeolian sediment transport. Land 2017;6(3):64. https://doi.org/10.3390/land6030064.
[58] Ikhwan M, Ruck B. Flow and pressure field characteristics around pyramidal buildings. J Wind Eng Ind Aerodynam 2006;94(10):745–65. https://doi.org/10.1016/j.jweia.2006.02.005.
[59] McKenna Neuman C, Sanderson RS, Sutton S. Vortex shedding and morphodynamic response of bed surfaces containing non-erodible roughness elements. Geomorphology 2013;198:45–56. https://doi.org/10.1016/j.geomorph.2013.05.011.
[60] Watson A. The control of windblown sand and moving dunes: a review of the methods of sand control in deserts, with observations from saudi arabia. Quart J Eng Geol 1985;18:237–52. https://doi.org/10.1144/GSL.QJEG.1985.018.03.05.
[61] Luo W, Dong Z, Qian G, Lu J. Near-wake flow patterns in the lee of adjacent obstacles and their implications for the formation of sand drifts: a wind tunnel simulation of the effects of gap spacing. Geomorphology 2014;213:190–200. https://doi.org/10.1016/j.geomorph.2014.01.008.
[62] Luo W, Lu J, Qian G, Dong Z. Influence of the gap ratio on variations in the surface shear stress and on sand accumulation in the lee of two side-by-side obstacles. Environ Earth Sci 2016;75:766. https://doi.org/10.1007/s12665-016-5588-3.
[63] Unnikrishnan S, Ogunremi A, Sumner D. The effect of incidence angle on the mean wake of surface-mounted finite-height square prisms. Int J Heat Fluid Flow 2017;66:137–56. https://doi.org/10.1016/j.ijheatfluidflow.2017.05.012.
[64] Ozmen Y, Baydar E, van Beeck J. Wind flow over the low-rise building models with gabled roofs having different pitch angles. Build Environ 2016;95:63–74. https://doi.org/10.1016/j.buildenv.2015.09.014.
[65] Qi W, Gao F. Physical modeling of local scour development around a large-diameter monopile in combined waves and current. Coast Eng 2014;83:72–81. https://doi.org/10.1016/j.coastaleng.2013.10.007.
[66] Gerwick Jr. B, Bittner R. Construction of marine and offshore structures. CRC Press; 2007.
[67] Sumner D. Flow above the free end of a surface-mounted finite-height circular cylinder: A review. J Fluids Struct 2013;43:41–63. https://doi.org/10.1016/j.jfluidstructs.2013.08.007.
[68] Cheng J, Xin G, Zhi L, Jiang F. Unloading characteristics of sand-drift in wind-shallow areas along railway and the effect of sand removal by force of wind. Sci Rep 7 (41462). https://doi.org/10.1038/srep41462.
[69] Xiao J, Qu J, Yao Z, Pang Y, Zhang K. Morphology and formation mechanism of sand shadow dunes on the Qinghai-Tibet Plateau. J Arid Land 2015;7(1):10–26. https://doi.org/10.1007/s40333-014-0074-9.
[70] Nathawat V, Sharda A. Challenges of track maintenance in desert area - problems and remedies. Permanent Way Bull 2005;32(1):1–8.
[71] Lehman C. Oregon Creates New Unit Of Government Just To Control Sand. <http://nwnewsnetwork.org/post/oregon-creates-new-unit-government-just-control-sand>; 2015.
[72] Kaushik. The Sand Buried Village of Shoyna. <http://www.amusingplanet.com/2016/07/the-sand-buried-village-of-shoyna.html>; 2016.
[73] Hao Y, Feng Y, Fan J. Experimental study into erosion damage mechanism of concrete materials in a wind-blown sand environment. Construct Build Mater 2016;111:662–70. https://doi.org/10.1016/j.conbuildmat.2016.02.137.
[74] Xue H, Shen X, Liu Q, Wang R, Liu Z. Analysis of the damage to the aeolian sand concrete surface caused by wind-sand erosion. J Adv Concr Technol 2017;15:724–37. https://doi.org/10.3151/jact.15.724.
[75] Liu L, Gao S, Shi P, Li X, Dong Z. Wind tunnel measurements of adobe abrasion by blown sand: profile characteristics in relation to wind velocity and sand flux. J Arid Environ 2003;53(3):351–63. https://doi.org/10.1006/jare.2002.1049.
[76] Zakeri JA, Forghani M. Railway route design in desert areas. Am J Environ Eng 2012;2(2):13–8. https://doi.org/10.5923/j.ajee.20120202.03.
[77] Indraratna B, Su L, Rujikiatkamjorn C. A new parameter for classification and evaluation of railway ballast fouling. Can Geotech J 2011;48(2):322–6. https://doi.org/10.1139/T10-066.
[78] Ionescu D, Fedele D, Trounce M, Petrolito J. Deformation and degradation characteristics of sand-contaminated railway ballast. In: Pombo J, editor. Proceedings of the third international conference on railway technology: research, development and maintenance, no. 26 Stirlingshire, UK: Civil-Comp Press; 2016. https://doi.org/10.4203/ccp.110.26.
[79] Faccoli M, Petrogalli C, Lancini M, Ghidini A, Mazzú A. Effect of desert sand on wear and rolling contact fatigue behaviour of various railway wheel steels. Wear 2018;396–397:146–61. https://doi.org/10.1016/j.wear.2017.05.012.
[80] Tyfour WR. Predicting the effect of grinding corrugated rail surface on the wear

behavior of pearlitic rail steel. Tribol Lett 2008;29(3):229–34. https://doi.org/10.1007/s11249-008-9300-y.
[81] Kóllmann J. Railway operations under harsh environmental conditions - sand, dust & humidity problems and technical solutions/mitigation measures. In: AHK Workshop Be a Partner of Qatar Rail, Berlin; 2013. URL <http://docplayer.net/22407097-Railway-operations-under-harsh-environmental-conditions.html>.
[82] Raffaele L, Bruno L, Pellerey F, Preziosi L. Windblown sand saltation: a statistical approach to fluid threshold shear velocity. Aeolian Res 2016;23:79–91. https://doi.org/10.1016/j.aeolia.2016.10.002.
[83] Raffaele L, Bruno L, Wiggs GF. Uncertainty propagation in aeolian processes: from threshold shear velocity to sand transport rate. Geomorphology 2018;301:28–38. https://doi.org/10.1016/j.geomorph.2017.10.028.
[84] Lettau K, Lettau H. Experimental and micro-meteorological field studies of dune migration. Tech. Rep. 101, 110-147, Exploring the World's Driest Climate (IES Report, 101, 110-147); 1978.
[85] Melcher ER, Beck AT. Structural reliability analysis and prediction. Wiley; 2018.
[86] Edgell HS. Arabian desert. Springer; 2006.
[87] Burlando M, De Gaetano P, Pizzo M, Repetto M, Solari G, Tizzi M. Wind climate analysis in complex terrain. J Wind Eng Ind Aerodynam 2013;123:349–62. https://doi.org/10.1016/j.jweia.2013.09.016.
[88] Hotta S, Horikawa K. Function of sand fence placed in front of embankment. Coast Eng 1991;1990(2):2754–67. https://doi.org/10.1061/9780872627765.211.
[89] Repetto MP, Torrielli A. Long term simulation of wind-induced fatigue loadings. Eng Struct 2017;132:551–61. https://doi.org/10.1016/j.engstruct.2016.11.057.
[90] Torrielli A, Repetto MP, Solari G. Long-term simulation of the mean wind speed. J Wind Eng Ind Aerodynam 2011;99:1139–50. https://doi.org/10.1016/j.jweia.2011.08.003.